Self-Assembly of ABC Star Triblock Copolymers under a Cylindrical Confinement

Yuci Xu, Weihua Li,* Feng Qiu, and Yuliang Yang

The Key Laboratory of Molecular Engineering of Polymers, Ministry of Education, China, Department of Macromolecular Science, Fudan University, Shanghai 200433, China

An-Chang Shi

Department of Physics and Astronomy, McMaster University, Hamilton, Ontario, Canada, L8S 4M1

Received: May 11, 2009; Revised Manuscript Received: June 28, 2009

Self-assembly of ABC star triblock copolymers confined in cylindrical nanopores is studied using real-space self-consistent mean-field theory. Specifically, the investigation focuses on the confined self-assembly of a triblock copolymer which forms hierarchical lamellae in the bulk. Generically, the hierarchical lamellae can be parallel or perpendicular to the pore surfaces. Concentric rings of A and B/C lamellae are formed in the parallel case. The B/C layers further form B/C domains. The number of B/C domains is controlled by the pore size. In the perpendicular case, the B/C layers are arranged alternatively along the pore axis. The stability of these observed structures is analyzed.

I. Introduction

The self-assembly of block copolymers in confined space has attracted tremendous attention in recent years. Introducing geometric confinement is viewed as an alternative method of fabricating novel nanoscale ordered structures, as compared with changing the chemical components, or interactions between immiscible species, or architectures of block copolymers. The simplest case of symmetric confinement is in the form of thin films, or one-dimensional confinement. It has been demonstrated that the thickness and surface interaction provide an effective method to control the orientation of the self-assembled structures in the one-dimensional case.[1−4] In recent years, higher-dimensional geometric confinements have received intensive interest because they add richer physics into block copolymer systems.[5−7] A typical two-dimensional (2D) confinement is in a cylindrical nanopore, and a three-dimensional (3D) confinement is in a spherical cavity.[8−11]

In the past several years, many authors have studied the self-assembly of block copolymers confined in a cylindrical pore in experiments and in theories.[12−25] In experiments done by Russell's group,[14] a polystyrene-*b*-polybutadiene (PS-*b*-PBD) diblock copolymer melt was loaded into cylindrical alumina nanopores. It was observed to self-assemble into many novel structures after annealing. For a nearly symmetric diblock copolymer, these structures include concentric lamellae with different numbers of layers, depending on the pore size. For an asymmetric diblock copolymer (cylinder formation in the bulk), these structures include straight cylinders along the pore axis in large pores and helices in narrow pores. A similar system has also been modeled and studied intensively by Monte Carlo (MC) simulations,[17,21−23,26] dynamical density functional (DDF) simulations,[18,25] and self-consistent mean-field theory (SCMFT).[19,20,26] The early work started from the simple case of symmetric diblock copolymers in a nanopore, by He et al.[17] and Sevink et al.[18] These authors observed concentric lamellae for preferential surface field and perpendicular lamellae for neutral pores. Motivated by the experiments, Li and Wickham first systematically studied the cylindrically confined diblock copolymer system by using the real-space method of SCMFT in two-dimensional space,[19] resulting in more than 20 2D equilibrium structures. In a subsequent work,[20] Li and Wickham extended the SCMFT calculations to 3D space. They found a few interesting novel 3D structures including stacked disks, single helix, double helices, toroids, and so on. These 3D structures follow a universal transit sequence as the pore size is varied. Those results are consistent with those of MC simulations done by Yu et al.[21] Recent work done by Sevink and Zvelindovsky suggests that a lot of exotic 3D structures, such as helical structures and perforated lamellae, can also be formed in nearly symmetric diblock copolymers confined in pores.[25] By adjusting the length of the pores, they find that most of these exotic structures are metastable.

Diblock copolymers are the simplest type of block copolymers. It is natural to expect that richer phase behavior will be found in a more complex type of block copolymers. Indeed, when the number of distinct blocks is increased from two, the complexity and variety of self-assembled structures are significantly increased.[27,28] In particular, it has been shown experimentally and theoretically that a simple extension of AB diblock copolymers to ABC triblock copolymers leads to a very large number of new morphologies.[27,29,30] For ABC triblock copolymer, there are two possible topological architectures: linear and star. The self-assembly behavior of these triblock copolymers is very different.[29−32] It is expected that confined self-assembly of ABC triblock copolymers will lead to new phenomena. For linear ABC triblock copolymers, a few groups have investigated their self-assembly in nanopores. For cylindrical confinement, Li's group has studied ABA triblock copolymers[33] and Liang's group[35] and Feng et al.[34] have investigated ABC linear triblock copolymers. On the other hand, studies on ABC star triblock copolymer under cylindrical confinement are lacking.

Before studying the structures of ABC triblock copolymers under confinement, it is necessary to understand their phase behavior in the bulk. Gemma et al. have proposed that ABC star copolymers self-assemble into cylindrical phases of tiling patterns when the three components are immiscible and the three

* Corresponding author. E-mail: weihuali@fudan.edu.cn.

10.1021/jp9043896 CCC: $40.75
Published on Web 07/20/2009

arms are long enough to give stable three-phase structures.[36] They found that a few two-dimensional structures of tiling patterns exist for a series of polymers of the type $A_{1.0}B_{1.0}C_x$, with x ranging from about 0.4 to 2.5. These morphologies were observed by Matsushita's group in subsequent experiments.[28] Theoretically, Tang et al. have examined the self-assembly of ABC star copolymer melts in bulk by means of SCMFT calculations in 2D space, and observed similar structures.[32] One of those interesting structures is the hierarchical lamella which is composed of an A layer and B/C layer, in which the B and C blocks further separate to form B/C domains. Two periods are required to characterize the structure: one is for the distance between two neighbor A layers, and another is for the B/C domain repeating size. When a cylindrical confinement is imposed on this ABC star triblock copolymer, its self-assembly becomes more complicated than in the bulk. Therefore, confined self-assembly of ABC triblock copolymers presents a very interesting case, in which the hierarchical structure is competing with the confinement effects. The present work focuses on the study of this cylindrically confined ABC star triblock copolymer, which forms hierarchical lamellar structure in bulk. Equilibrium microstructures are explored for various pore diameters, and their stability regions as a function of the pore diameter are identified by comparing their free energy. In order to calculate the free energy accurately, we employ the self-consistent mean-field theory in our study. In our study, solutions of SCMFT equations corresponding to different structures are obtained, and then, the free energy density of candidate structures is used to construct their phase diagram.

II. Theory

We consider an incompressible melt of ABC star triblock copolymers, confined in a cylindrical pore of diameter D. Each copolymer has a degree of polymerization N, and the chain lengths of A, B, and C blocks are f_AN, f_BN, and f_CN ($f_A + f_B + f_C = 1$), respectively. Spacial lengths in our calculations are expressed in units of the radius of gyration, R_g, of the polymer. Within the mean-field approximation to the many-chain Edwards theory,[37−40] at a temperature T, the free energy F for n Gaussian diblock copolymer chains confined in a cylindrical pore has the form

$$\frac{F}{nk_BT} = -\ln Q + \frac{1}{V}\int_{|\mathbf{r}|\le R} d\mathbf{r}\{\chi_{AB}N\phi_A(\mathbf{r})\phi_B(\mathbf{r}) + \chi_{AC}N\phi_A(\mathbf{r})\phi_C(\mathbf{r}) + \chi_{BC}N\phi_B(\mathbf{r})\phi_C(\mathbf{r}) - \omega_A(\mathbf{r})\phi_A(\mathbf{r}) - \omega_B(\mathbf{r})\phi_B(\mathbf{r}) - \omega_C(\mathbf{r})\phi_C(\mathbf{r}) + H(\mathbf{r})[\phi_A(\mathbf{r}) - \phi_B(\mathbf{r}) - \phi_C(\mathbf{r})]\} \quad (1)$$

where ϕ_A, ϕ_B, and ϕ_C are the monomer densities. The partition function Q is for a single polymer interacting with the mean fields ω_A, ω_B, and ω_C produced by the surrounding chains. The interactions among the three dissimilar monomers are characterized by three Flory−Huggins interaction parameters, χ_{AB}, χ_{AC}, and χ_{BC}. In the confined melts, the spatial integration is restricted to the pore volume, taken to be V. The preference of the pore wall is introduced by including a surface field $H(\mathbf{r})$ in eq 1. Similar to our previous work,[19,20] this surface field is chosen to have the form

$$\frac{H(\mathbf{r})}{\chi N} = V_0\{\exp[(\sigma + |\mathbf{r}| - R)/\lambda] - 1\} \quad (2)$$

for $R - \sigma \le |\mathbf{r}| \le R$, while $H(\mathbf{r}) = 0$ for $|\mathbf{r}| < R - \sigma$. In this work, we chose the cutoff distance for the surface interaction to be $\sigma = 0.5R_g$, and the decay length to be $\lambda = 0.25R_g$. $V_0 = 0$ means that the pore wall has no preference to any block. The pore wall prefers B and C for $V_0 > 0$ and prefers A for $V_0 < 0$.

Minimization of the free energy with respect to the monomer densities and the mean fields leads to the following standard mean-field equations[38]

$$\begin{aligned}
\omega_A(\mathbf{r}) &= \chi_{AB}N\phi_B(\mathbf{r}) + \chi_{AC}N\phi_C(\mathbf{r}) + H(\mathbf{r}) + \eta(\mathbf{r})\\
\omega_B(\mathbf{r}) &= \chi_{AB}N\phi_A(\mathbf{r}) + \chi_{BC}N\phi_C(\mathbf{r}) - H(\mathbf{r}) + \eta(\mathbf{r})\\
\omega_C(\mathbf{r}) &= \chi_{AC}N\phi_A(\mathbf{r}) + \chi_{BC}N\phi_B(\mathbf{r}) - H(\mathbf{r}) + \eta(\mathbf{r})\\
\phi_A(\mathbf{r}) &= \frac{1}{Q}\int_0^{f_A} ds\, q_A(\mathbf{r}, s)q_A^\dagger(\mathbf{r}, s)\\
\phi_B(\mathbf{r}) &= \frac{1}{Q}\int_0^{f_B} ds\, q_B(\mathbf{r}, s)q_B^\dagger(\mathbf{r}, s)\\
\phi_C(\mathbf{r}) &= \frac{1}{Q}\int_0^{f_C} ds\, q_C(\mathbf{r}, s)q_C^\dagger(\mathbf{r}, s)\\
Q &= \frac{1}{V}\int d\mathbf{r}\, q_K(\mathbf{r}, s)q_K^\dagger(\mathbf{r}, s) \qquad (3)
\end{aligned}$$

$$\phi_A(\mathbf{r}) + \phi_B(\mathbf{r}) + \phi_C(\mathbf{r}) = 1 \quad (4)$$

In the above equations, $q_K(\mathbf{r}, s)$ and $q_K^\dagger(\mathbf{r}, s)$ (K = A, B, C) are end-segment distribution functions. The distribution function $q_K(\mathbf{r}, s)$ is proportional to the probability that a polymer chain segment, of contour length s and with one free end, has its other end located at $\mathbf{r}$. These distribution functions satisfy the modified diffusion equations

$$\frac{\partial q_K(\mathbf{r}, s)}{\partial s} = \nabla^2 q_K(\mathbf{r}, s) - \omega_K(\mathbf{r}, s)q_K(\mathbf{r}, s) \quad (5)$$

$$-\frac{\partial q_K^\dagger(\mathbf{r}, s)}{\partial s} = \nabla^2 q_K^\dagger(\mathbf{r}, s) - \omega_K(\mathbf{r}, s)q_K^\dagger(\mathbf{r}, s) \quad (6)$$

The initial conditions are $q_K(\mathbf{r}, 0) = q_L^\dagger(\mathbf{r}, 0)q_M^\dagger(\mathbf{r}, 0)$, where $(KLM) \in \{(ABC), (BCA), (CAB)\}$, and $q_K^\dagger(\mathbf{r}, f_K) = 1$. For numerical solution, we employ the split-step Fourier method of Tzeremes et al.[41,42] to solve the modified diffusion equations for the end-segment distribution functions. Similar to our previous work,[19,20] the cross section of the pore is put in a rectangular cell which is a little larger than the diameter of the pore. In the split-step Fourier method, periodic boundary conditions are imposed automatically on the square cell. In our calculations, we discretize the cell into $N_x \times N_y = 128 \times 128$ lattices, and the contour length is divided into 64 segments for each block. For three-dimensional calculations, $N_z = 64$ points are used for the third dimension.

In this system, there are seven parameters, χ_{AB}, χ_{AC}, χ_{BC}, f_A, f_B, D, and V_0, controlling the phase behavior. In this work, we restrict ourselves to a few typical parameter groups. For a given set of parameters, we first use random initial conditions for the mean fields in our iterative algorithm to generate a set of solutions to the mean-field equations. Once we determine a set of solutions to the mean-field equations, we then use these solutions as initial conditions in our algorithm to obtain their free energy which is used to identify their stability of the structures.

III. Results and Discussion

As our investigation focuses on a star triblock copolymer which forms a hierarchical lamellar phase in the bulk, we chose

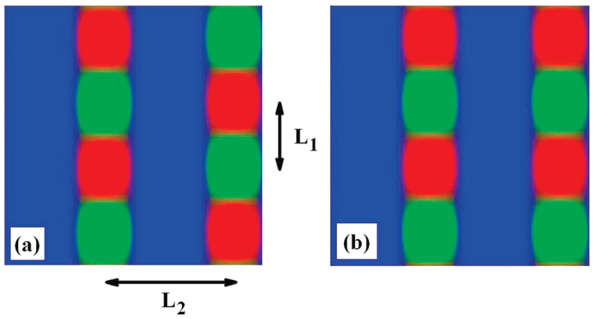

Figure 1. Monomer density plots of the bulk phase formed in the melts of ABC star triblock copolymer with $\chi_{AB}N = \chi_{AC}N = \chi_{BC}N = 60$, $f_A = 0.6$, $f_B = 0.2$, and $f_C = 0.2$. The colors of blue, red, and green indicate the regions where the greatest component is A, B, and C, respectively. L_1 is the period of alternating B/C domains, and L_2 is the distance between two neighboring A-domain layers. Parts a and b show two cases of B/C sequences for two neighboring layers: B/C domains are arranged with $L_1/2$ shift in part a and with no shift in part b.

its volume fractions as $f_A = 0.6$ and $f_B = f_C = 0.2$, and with fixed repulsive interactions $\chi_{AB}N = \chi_{AC}N = \chi_{BC}N = 60$. The strength parameter of the surface field is chosen as $V_0 = -0.20$ to give strong attraction to the A block and strong repulsion to the B and C blocks. Figure 1 shows the monomer density plots formed by the copolymer melt in bulk obtained by real-space SCMFT calculations. The three colors of blue, green, and red represent the regions where the greatest component is A, B, and C, respectively. Obviously, the bulk microphase is a typical hierarchical lamellar phase which consists of A-domain lamellae and alternating-B/C-domain-formed lamellae (denoted as LAM+BD by Tang et al.[32]). Here, two lengths are used to characterize its periodicity. One, indicated by L_1 in Figure 1a, is used to measure the period of alternating B/C domains, and the other one shown as L_2 is used to measure the distance between two neighboring A-domain layers. For the chosen set of parameters, the two periods are determined as $L_1 = 2.532R_g$ and $L_2 = 4.260R_g$ (R_g is the radius of gyration of the copolymer) by SCMFT calculations. In our real-space SCMFT calculations, as random initial fields are used to start the iteration of the SCMFT equations, more than one solution can be obtained. Figure 1b shows another possible equilibrium morphology different from that in Figure 1a. In Figure 1a, two neighboring B/C-domain-formed lamellae have a half-period shift of $L_1/2$, and in Figure 1b, there is no shift. It is intuitively thought that the morphology of Figure 1a has lower free energy than that of Figure 1b. By calculating the free energy difference of a morphology with varied shifts between zero and $L_1/2$, we find that the free energy difference, as a function of the shift, depends on the Flory−Huggin interactions and the volume fractions. Generally, when the interactions $\chi_{AB}N = \chi_{AC}N < \chi_{BC}N$, the free energy difference decreases as the shift increasing. This means that the morphology of Figure 1a has the lowest free energy as expected. The magnitude of the free energy difference becomes larger when $\chi_{AB}N = \chi_{AC}N$ decreases for a fixed $\chi_{BC}N$. This is caused by the increased width of the interface between A and B/C domains and the decreased distance between two neighboring interfaces. Oppositely, the free energy difference becomes smaller. This suggests that the free energy tends to be independent of the shifting when the interactions of $\chi_{AB}N = \chi_{AC}N$ become large enough. In consequence, the system can have an infinite number of degenerate states, as any pair of neighboring B/C layers can have any shift. For the choice of $\chi_{AB}N = \chi_{AC}N = \chi_{BC}N = 60$, the free energy difference between the two morphologies in Figure 1 is very tiny (much smaller than 10^{-4}). As the present work focuses on the confined system where the arrangement of domains is very different from that in the bulk, we do not discuss it much here. More details about the free energy of the bulk phase will be presented in our future work.

For the star triblock copolymers confined in cylindrical nanopores, many equilibrium solutions of the SCMFT equations for the fixed set of parameters are obtained by the application of varied random initial fields. The stability of each structure is examined by comparing its free energy with other candidate structures. As the bulk phase of this triblock copolymer is a hierarchical lamellar phase, there is a tendency for it to self-assemble into hierarchical concentric lamellar structures under the confinement of a nanopore with preferential interactions to one block similar to the self-assembly in cylindrically confined diblock copolymers (CCDBCP). For the investigation of this kind of structure, we can perform our SCMFT calculations in two-dimensional space. A typical free energy comparison among a few structures is presented in Figure 2a. The monomer density plots of these structures are shown in Figure 2b, and their relative stability regions as a function of diameter D are plotted in Figure 2c for $f_A = 0.6$ and $f_B = f_C = 0.2$. The diameter is rescaled in units of the period L_2 in bulk. Figure 2d shows the density profiles of structures and corresponding stability regions for larger pores. For convenience, structures shown in Figure 2b are denoted as P_n, where n indicates the repeating number of BC domains except for the case of P_2. The structures of P_n ($n = 5$ to $n = 9$) with n-fold symmetry are typical hierarchical concentric lamellar structures with a B/C-alternating-domains co-formed concentric layer like their bulk counterpart. Their repeating number of BC domains increases from 5 to 9 as the diameter is increased. The number of BC domains is determined by the average domain size on the ring. The average domain sizes of structures P_n, which can be estimated by dividing the circumference of the ring at the center of the BC domain along the pore radius by the number of BC domains, are given in Figure 3. L is rescaled with the bulk value of BC-domain size $L_1 = 2.532R_g$. The dashed lines are used to indicate the transitions between two neighbor phases. We can see that more BC domains are added to relax the stretching energy when their average size is much larger than the bulk value.

For the single-ring structures of P_n, the stretching energy and interfacial energy have the best balance when the pore diameter is just above twice of the natural period L_2 in bulk as the effect of the pore curvature.[43] In Figure 2, the structures P_7 and P_8 satisfy this condition. As the pore size is decreased, the interfacial area of A/B and A/C domains is increased as the domains along the radial direction are compressed. For smaller diameters than that of P_5, the interfacial energy becomes very high if the single-ring structure remains. P_4 is not formed to continue the structure sequence, and it is replaced by P_3 which consists of a hexagonal C domain at the center and three petals of BC domains around when $D/L_2 < 1.62$. In the structure P_3, the interfacial area between A and B/C domains is decreased by breaking the B/C coformed ring. When the pore size is decreased further, the compression of the domain sizes induces the interfacial energy to become high again. As the number of domains are enforced to be reduced, P_2 is formed to replace P_3. For very narrow pores, i.e., $D/L_2 < 1.2$, the structure of P_1 only composed of concentric layers is formed. In those mentioned structures, we should notice that B and C blocks are symmetric, as they have the same volume fractions for our choice of parameters. The two components in these structures can be switched to form complementary equilibrium structures

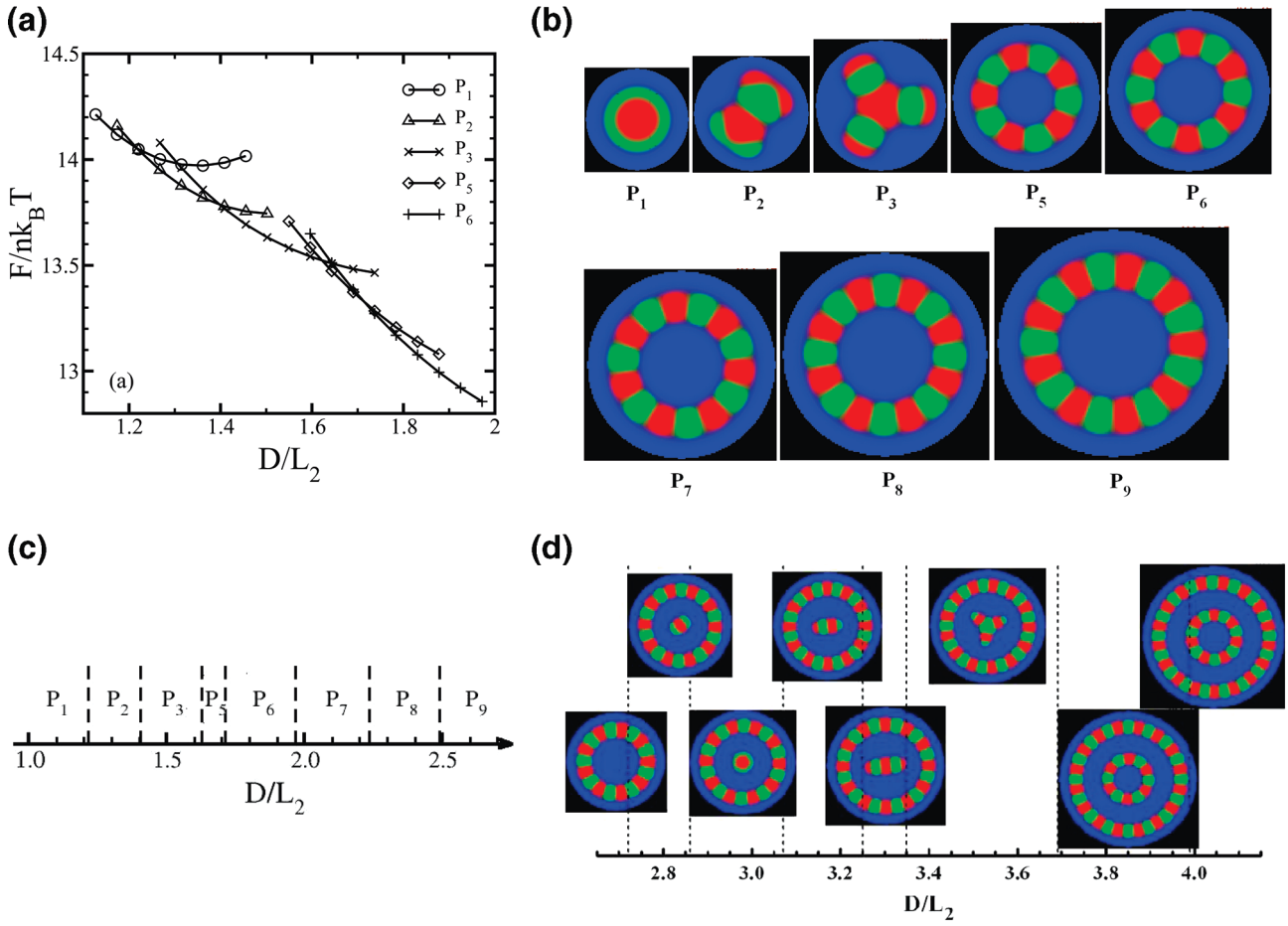

Figure 2. (a) Typical free energy curves of a few structures observed in the ABC star triblock copolymer melts, with $f_A = 0.6$ and $f_B = f_C = 0.2$, under the confinement of cylindrical pores for varied diameters D, which is rescaled in units of the period L_2. The pore wall attracts A and repulses B and C. The monomer density profiles of these structures are shown in part b. The stability regions of these structures obtained by comparing their free energy for narrower pores is plotted in part c, and that for larger pores is plotted in part d. Blue, green, and red represent A, B, and C domains, respectively.

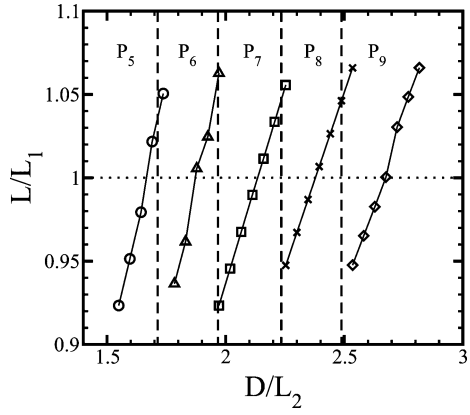

Figure 3. Width of two neighboring B and C domains at the domain center along the pore radius as a function of the pore diameter D. The width and pore diameter are rescaled by periods L_1 and L_2, respectively.

with the same free energy. In the regions of narrow pores, it is possible for BC domains to be arranged along the pore axis to form three-dimensional structures. We will discuss this later. The structure sequence P_n is not continued when the pore size is larger than that of $n = 9$, either. It is because the stretching energy of A blocks becomes high in the single-ring structures as the diameter is increased. Some domains appear at the center of the pore to release the high stretching of A blocks. More possible structures can be formed by two means of varying the inner part, or adding of BC domains into the outer ring. In our 2D calculations, four structures are observed with different inner parts when D is increased: three-layer, concentric lamellae, four-layer, and P_3. When the diameter is increased to be larger than $D/L_2 > 3.7$, the structures with double BC-domain rings appear. The mechanism of varying the layers of the structures for varied pore size is similar to that during the formations of concentric lamellae of the CCDBCP system. In our previous work,[43] we studied the self-assembly behavior of near symmetric diblock copolymers confined in cylindrical pores. Our results indicate that the transitions among concentric lamellae are at the pore size larger than the integer time of the bulk period because of the effect of the interface curvature induced by the pore wall. The single-ring structures exist until $D/L_2 > 2.72$.

The above results are from the self-assembly of the ABC star copolymer melts confined in pores with pore-wall preference to the largest block. According to previous work,[19−21,25] the preference of the pore wall also has a significant influence on the structure formation of the copolymers. Here, we still use the compositions as (0.6, 0.2, 0.2), but we change the composition sequence as the block attracted by the pore wall to be $f_A = 0.2$, and set the other two repulsed blocks as $f_B = 0.2$ and $f_C = 0.6$. Figure 4 presents the observed structures and their stability regions as a function of the pore diameter. The inner parts of these structures are similar to the structures observed in the case where the pore wall prefers the largest block. The reason for the formation of the outer layers near the pore wall is similar

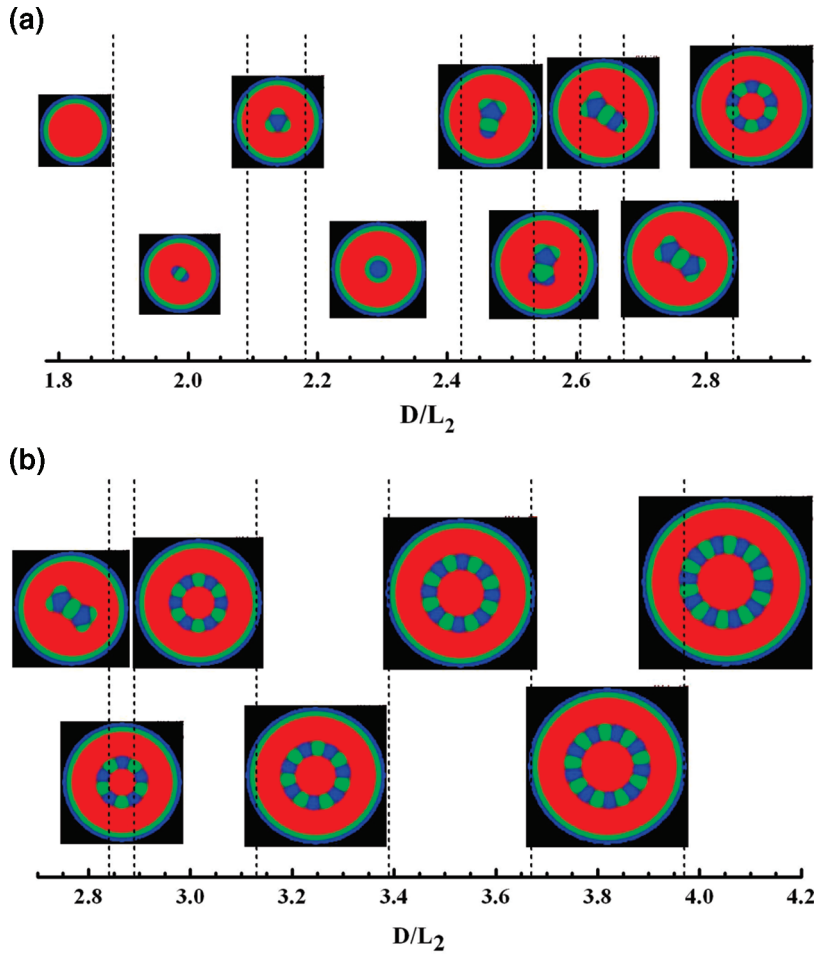

Figure 4. Phase diagrams of the structures formed by copolymers with $f_A = f_B = 0.2$ and $f_C = 0.6$ in nanopores with varying diameter. The pore wall has attractive preference to the A component and repulsion to the B and C components.

to that in the CCDBCP system.[19] The pore wall attracts small block A to form a thin layer close to the wall, and small block B is enforced to form a neighbor thin layer by their connection. Inside of the two thin layers, the largest block C is arranged. In the inner space, the structures are formed according to the way in which the larger block C stays outside of the interface, and the smaller blocks A and B stay inside of the interface. An overbar is used to denote these single-ring structures as $\bar{P}_n$ in this case. Compared with the other case in Figure 2, the structure sequence has a shift accounting for the narrower effective pore. The shifts for different transitions have a small dependence on the pore diameter, and are almost constant during the narrow region. For example, the shifts are around $1.2L_2$ in the region from P_5 to P_9.

Similar to the CCDBCP system, there is another possible way for the copolymer to form microstructures. When considering the pore wall with a strong preference to the largest block A, A blocks are attracted to form a concentric layer near the wall. Novel structures, different from the 2D structures, can be formed by changing the arrangement of B/C domains, i.e., arranging B and C domains alternatively along the pore axis. In order to examine the formation of this kind of structure, we extend our 2D calculations to three-dimensional space. According to the knowledge from the CCDBCP system, understanding self-assembling behaviors in the narrow-pore region, where single-layer structures are formed, is crucial to understanding the confinement effect of larger pores. Therefore, we concentrate our 3D calculations to the small-pore-size region. A few 3D equilibrium structures, different from the 2D structures given above, are observed in this region. These 3D structures (Figure 5) are stacked disks, stacked 3-fold lobes, stacked 4-fold lobes, and stacked rings. These four structures are denoted as *Dk*, Lb_3, Lb_4, and *Rn*, respectively. The 3D structures are periodic along the pore axis. The work in the CCDBCP system tells us that the free energy is a function of the pore length for these periodic structures.[20,25] Therefore, we minimize the free energy by adjusting the pore length to zero the extensional forces.[25] We find that the periods of these structures, only with slight dependence on the pore size (smaller than 0.5%), are close to the bulk period of L_1. This suggests that the size of repeating B/C domains is hardly influenced by the confinement.

Figure 5. Monomer density plots of four three-dimensional structures. The isodensity surfaces of $\phi_k = 0.5$ (k = A, B, and C) are shown in blue, red, and green colors. From left to right, these structures are stacked disks (denoted as *Dk*), stacked 3-fold lobes (denoted as Lb_3), stacked 4-fold lobes (denoted as Lb_4), and stacked rings (denoted as *Rn*).

In the 2D structures, the junction points of the three arms align in a straight line parallel to the pore axis to keep the translational symmetry like their bulk behaviors. However, in 3D structures, the translational symmetry is broken when B and C domains are arranged along the pore axis. From these

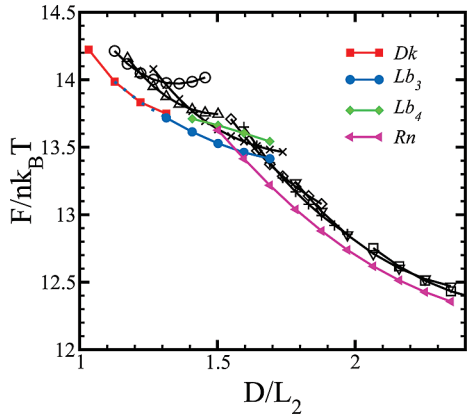

Figure 6. Comparisons of the free energy between two-dimensional structures and three-dimensional structures. The hollow symbols are the free energy of 2D structures P_k (k = 1, 2, ..., 8), and the filled symbols are the free energy of 3D structures: stacked disks, stacked 3-fold lobes, stacked 4-fold lobes, and stacked rings. The dotted line is the extrapolation of the free energy curve of Lb_3 toward that of stacked disks.

structures in Figure 5, we find that the junction points form a curve in a plane perpendicular to the pore axis. The junction-point-formed curve can be circles, 3-fold lobes, and 4-fold lobes. In order to analyze their stability compared with 2D structures, we calculate their minimal free energy at equilibrium, and compare their free energy among themselves, also with those of 2D structures in Figure 6. From the comparison of the free energy, we can conclude that the 3D structures have lower free energy than the corresponding 2D structures appearing in their phase diagram in Figure 2. This suggests that the 3D structures become stable structures instead of 2D structures. The difference of the free energy between the 2D structures and the 3D structures has a decreasing tendency as the pore diameter increases. This is due to the effect of the curvature imposed on the microstructures by the geometrical confinement. In the 2D ring structures, B and C domains are packed in a similar way as those in bulk except that their alignment is in a circle path different from the straight path in bulk. When the pore size becomes larger, the circle path with smaller curvature is closer to the straight one. This predicts that it might be easier to observe 2D ring structures in experiments for larger pores when the wall preference is present.

From the results of free energy, we can see that the stable structure sequence is *Dk*, Lb_3, and *Rn* as increasing pore size, and the structure Lb_4 is a metastable structure. In these 3D structures, packing B/C repeating domains along the pore axis allows the BC-domain size to be adjusted freely. For the arrangement of B/C domains, it is similar as the perpendicular lamellae in the CCDBCP system. However, the junction among A/B/C blocks induces restriction on the B/C domain size along the radial direction. For very narrow pores, stacked disks are the preferred stable structure. Without considering the separation between B and C, the structure is similar to the single-cylinder structure in the CCDBCP system. When the pore diameter becomes larger than the bulk period of L_2, i.e., $D > 1.2L_2$, an energy penalty is resulted by the stretching of B/C blocks from the junction-point circle to the center of B/C domains. One way to relax the stretching energy is to form a fluctuated junction-point circle (or A/B/C three-phase interface) with a cost of increasing interfacial energy, such as the curves with 3-fold or 4-fold lobes. The concave parts of the interfaces can reduce the stretching of B/C blocks to the domain center. Therefore, the formation of the 3D structures is also frustrated. The structure with 3-fold lobes reaches the best balance compared with stacked disks and the structure with 4-fold lobes for the region of $1.20L_2 < D < 1.56L_2$. In our calculations, we do not find a first-order transition between the structures *Dk* and Lb_3. It seems that the formation of three lobes from the disks should be a continuous process as the pore size is increasing. When the pore size is increased further, single-ring structures become stable for B/C domains. The stacked ring structure appears at a similar region ($D \approx 1.56L_2$) as that ($D \approx 1.61L_2$) where the first single-ring 2D structure of P_5 appears with the relatively low free energy among all 2D structures.

IV. Conclusions

In summary, we have studied the formation of microstructures in a cylindrically confined star triblock copolymer melt, which forms a hierarchical lamellar structure in bulk, by using real-space SCMFT. We have examined the formation of two possible kinds of microstructures in cylindrically confined ABC star triblock copolymers. One kind of structures are hierarchical concentric lamellae and some intermediate structures. These structures are 2D, and they have translational symmetry along the pore axis. Another kind of structures are formed by arranging B/C domains alternatively along the pore size when keeping A domains as a contacting layer on the wall because of the strong preference of the wall. For the small-pore-size region ($D/L_2 <$ 2.4), a few interesting structures, including stacked disks (*Dk*), stacked 3-fold lobes (Lb_3), stacked 4-fold lobes (Lb_4), and stacked rings (*Rn*), are observed. It is interesting that the three-arm junction points form a curve in these 3D structures instead of a straight line in 2D structures or in the bulk system. By analyzing their free energy, we find that 3D structures *Dk*, Lb_3, and *Rn* become stable in the phase diagram instead of 2D structures. The 3D structure with 4-fold lobes is metastable. In addition, the transition between *Dk* and Lb_3 seems to be a continuous transition.

The star triblock copolymers have complex self-assembling behaviors in bulk, so their self-assemblies under cylindrical confinement become more complicated. Our work with reduced parameters can hopefully give some understanding to this system, and can guide some experiments on this subject. Though all 2D structures observed in SCMFT calculations are metastable, they can be observed in experiments. Particularly, there is a bigger possibility to observe 2D structures in relatively larger pores by experiments because our results suggest that the difference of the free energy between 2D structures and 3D structures decreases as the pore size increases. Experiments are also expected to prove our prediction of a kind of 3D structures.

Acknowledgment. The authors would like to thank the High-end Computing Centre at Fudan University for computing resourses. This work was supported by the National Natural Science Foundation of China (Grant 20704010). W.L. gratefully acknowledges support from the Shanghai Pujiang Program (Program No. 08PJ1402000) and the Shanghai Educational Development Foundation.

References and Notes

(1) Matsen, M. W. *J. Chem. Phys.* **1997**, *106*, 771.
(2) Xu, T.; Hawker, C. J.; Russell, T. P. *Macromolecules* **2005**, *38*, 2802.
(3) Yang, Y. Z.; Qiu, F.; Zhang, H. D.; Yang, Y. L. *Polymer* **2006**, *47*, 2205.
(4) Sakurai, S.; Bando, H.; Yoshida, H.; Fukuoda, R.; Mouri, M.; Yamamoto, K.; Okamoto, S. *Macromolecules* **2009**, *42*, 2115.
(5) Darling, S. B. *Prog. Polym. Sci.* **2007**, *32*, 1152.

(6) Yu, B.; Li, B. H.; Jin, Q. H.; Ding, D. T.; Shi, A. C. *Macromolecules* **2007**, *40*, 9133.
(7) Pinna, M.; Guo, X. H.; Zvelindovsky, A. V. *Polymer* **2008**, *49*, 2797.
(8) Yu, B.; Li, B. H.; Jin, Q. H.; Ding, D.; Shi, A. C. *Macromolecules* **2007**, *40*, 9133.
(9) Jeon, S. J.; Yi, G. R.; Koo, C. M.; Yang, S. M. *Macromolecules* **2007**, *40*, 8430.
(10) Higuchi, T.; Tajima, A.; Motoyoshi, K.; Yabu, H.; Shimomura, M. *Angew. Chem., Int. Ed.* **2008**, *47*, 8044.
(11) Higuchi, T.; Tajima, A. K.; Yabu, H.; Shimomura, M. *Soft Matter* **2008**, *4*, 1302.
(12) Wu, Y.; Cehng, G.; Katsov, K.; Sides, S. W.; Wang, J.; Tang, J.; Fredrickson, G. H.; Moskovits, M.; Stucky, G. D. *Nat. Mater.* **2004**, *3*, 816.
(13) Shin, K.; Xiang, H.; Moon, S. I.; Kim, T.; McCarthy, T. J.; Russell, T. P. *Science* **2004**, *306*, 76.
(14) Xiang, H.-Q.; Shin, K.; Kim, T.; Moon, S. I.; McCarthy, T. J.; Russell, T. P. *Macromolecules* **2004**, *37*, 5660.
(15) Xiang, H.; Shin, K.; Kim, T.; Moon, S.; McCarthy, T. J.; Russell, T. P. *J. Polym. Sci., Part B: Polym. Phys.* **2005**, *43*, 3377.
(16) Sun, Y.; Steinhart, M.; Zschech, D.; Adhikari, R.; Michler, H.; Gösele, U. *Macromol. Rapid Commun.* **2005**, *26*, 369.
(17) He, X.; Song, M.; Liang, H.; Pan, C. *J. Chem. Phys.* **2001**, *114*, 10510.
(18) Sevink, G. J. A.; Zvelindovsky, A. V.; Fraaije, J. G. E. M.; Huinink, H. P. *J. Chem. Phys.* **2001**, *115*, 8226.
(19) Li, W.; Wickham, R. A.; Garbary, R. A. *Macromolecules* **2006**, *39*, 806.
(20) Li, W.; Wickham, R. A. *Macromolecules* **2006**, *39*, 8492.
(21) Yu, B.; Sun, P.; Chen, P.; Jin, Q.; Ding, D.; Li, B.; Shi, A.-C. *Phys. Rev. Lett.* **2006**, 138306.
(22) Chen, P.; He, X.; Liang, H. *J. Chem. Phys.* **2006**, *124*, 104906.
(23) Feng, J.; Ruchenstein, E. *Macromolecules* **2006**, *39*, 4899.
(24) Wang, Q. *J. Chem. Phys.* **2007**, *126*, 024903.
(25) Sevink, G. J. A.; Zvelindovsky, A. V. *J. Chem. Phys.* **2008**, *128*, 084901.
(26) Chen, P.; Liang, H. J.; Shi, A. C. *Macromolecules* **2007**, *40*, 7329.
(27) Abetz, V.; Simon, P. F. W. *Adv. Polym. Sci.* **2005**, *189*, 125.
(28) Matsushita, Y. *Macromolecules* **2007**, *40*, 771.
(29) Tyler, C. A.; Qin, J.; Bates, F. S.; Morse, D. C. *Macromolecules* **2007**, *40*, 4654.
(30) Guo, Z.; Zhang, G.; Qiu, F.; Zhang, H.; Yang, Y.; Shi, A.-C. *Phys. Rev. Lett.* **2008**, *101*, 028301.
(31) Tang, P.; Qiu, Feng.; Zhang, H.; Yang, Y. *Phys. Rev. E* **2004**, *69*, 031803.
(32) Tang, P.; Qiu, F.; Zhang, H.; Yang, Y. *J. Phys. Chem. B* **2004**, *108*, 8434.
(33) Wang, Z.; Li, B. H.; Jin, Q. H.; Ding, D. T.; Shi, A. C. *Macromol. Theory Simul.* **2008**, *17*, 86.
(34) Feng, J.; Ruckenstein, E. *J. Chem. Phys.* **2007**, *126*, 124902.
(35) Chen, P.; Liang, H. *J. Phys. Chem. B* **2008**, *112*, 1918.
(36) Gemma, T.; Hatano, A.; Dotera, T. *Macromolecules* **2002**, *35*, 3225.
(37) Shi, A.-C. In *Development in Block Copolymer Science and Technology*; Hamley, I. W., Ed.; Wiley: New York, 2004.
(38) Fredrickson, G. H. *The Equilibrium Theory of Inhomogeneous Polymers*; Oxford University Press: Oxford, U.K., 2006.
(39) Helfand, E. J. *J. Chem. Phys.* **1975**, *62*, 999.
(40) Hong, K. M.; Noolandi, J. *Macromolecules* **1981**, *14*, 727.
(41) Tzeremes, G.; Rasmussen, K. Ø.; Lookman, T.; Saxena, A. *Phys. Rev. E* **2002**, *65*, 041806.
(42) Rasmussen, K. Ø.; Kalosakas, G. J. *J. Polym. Sci., Part B: Polym. Phys.* **2002**, *40*, 1777.
(43) Li, W.; Wickham R. A. *Macromolecules*, in press.

JP9043896